

Scientific Paper

Doi: <http://dx.doi.org/10.1590/1809-4430-Eng.Agric.v43n5e20230104/2023>

CROP DISEASE AND PEST IDENTIFICATION TECHNOLOGY BASED ON ACPSO-SVM ALGORITHM OPTIMIZATION

Zhigui Dong^{1*}, Yanchao Wang¹

^{1*}Corresponding author. School of Electronic and Information Engineering, Liaoning Institute Science and Technology/Benxi, China. E-mail: dongzhigui@163.com | ORCID ID: <https://orcid.org/0000-0002-4168-7991>

KEYWORDS

chaotic particle swarm, crops, diseases, characteristics, image.

ABSTRACT

Research on the classification and identification of crop diseases and pests can help farmers quickly prevent crop diseases and pests. A crop disease and pest identification model based on adaptive chaotic particle swarm optimization algorithm is raised. The model introduces swarm intelligence algorithm to optimize the features of image extraction. Then the adaptive inertia weight is used to improve the optimization performance of PSO, and the support vector is used to accurately classify crop pests and diseases. Finally, the model is trained by simulation experiment to evaluate the performance of the model and analyze the performance. The model has a good performance in the experiment, the model has a clear recognition effect in the color feature extraction of pests and diseases, and the recognition accuracy is 95.08% after combining the texture feature. Moreover, in the visual transformation of 20° -40° , the recognition accuracy of the model is above 90%. In practical application, the average accuracy of the model is 91.78%, which is 3.71% higher than that of the comparison algorithm. In comparison experiments, the classification accuracy of the proposed models is above 90%. The experimental outcomes denote that the proposed algorithm has good effectiveness in identifying crop diseases and pests.

INTRODUCTION

Crop pests and diseases are important problems in agricultural production, which pose a serious threat to the yield and quality of agricultural products. Traditional pest control methods mainly rely on manual observation and empirical judgment, and there are problems such as heavy workload, low efficiency and low precision. With the development of machine vision technology, especially the application of image processing and pattern recognition technology, the classification and recognition of crop pests and diseases have been gradually improved. Aiming at the complexity and challenge faced by the classification and recognition task of crop pests and diseases, an image recognition model combining adaptive chaotic particle swarm optimization algorithm and support vector machine was proposed (Xia et al., 2022; Guo et al., 2022). The model uses swarm intelligence algorithm and image processing technology to identify and prevent crop pests and diseases, and has the following technical routes: data collection and preprocessing, by collecting a large number

of crop diseases and pests image data, and preprocessing, including image denoising, image enhancement and image standardization and other steps. These steps are designed to reduce noise and interference in the data and improve the performance of subsequent classification models. Feature extraction and selection, the use of image processing technology to extract image features, such as texture features, shape features and color features. At the same time, the feature selection algorithm is used to select the most discriminative feature subset to reduce the dimension and improve the classification effect. Adaptive chaotic particle swarm optimization algorithm is introduced to optimize parameters and feature weights of support vector machine model (Dagal et al., 2022; Qteat & Awad, 2021). The algorithm can adjust the search strategy adaptively according to the local and global information in the optimization process, and improve the performance and stability of the classification model. Support vector machine classification model, using the optimized support vector machine classifier to classify crop pests and diseases. Support vector machine (SVM) is a classical

¹ School of Electronic and Information Engineering, Liaoning Institute Science and Technology/Benxi, China.

Area Editor: Gizele Ingrid Gadotti

Received in: 7-19-2023

Accepted in: 10-23-2023



machine learning algorithm with excellent classification and generalization ability, which is suitable for classification and identification of pests and diseases in complex scenarios. Through the above technical route, the research aims to quickly prevent the occurrence of crop diseases and pests, treat diseases and pests in a targeted way, reduce the pollution of pesticides on agricultural products and the environment, and improve crop yield, which has important agricultural practical significance.

The research analyzes the proposed model, and the research structure is mainly composed of four parts. The first part is to summarize the research on image recognition technology and crop pest identification technology by domestic and foreign scholars, and analyze their achievements and shortcomings; The second part is to construct and analyze the proposed model, and introduce the improvement methods and feature extraction of the model; The third part is to assess the effectiveness of comparative experiments and practical applications; The fourth part summarizes the experimental results, points out the shortcomings in the research, and proposes future research directions.

The use of machine vision related technologies for automatic identification of CDP can quickly and accurately provide identification results, overcoming the high misjudgment rate caused by subjectivity in traditional manual recognition. From the existing research results, its research mainly includes particle swarm optimization (PSO) algorithm and image feature extraction methods. Amiri A et al. proposed an adaptive Shewhart type control chart, and used the tuned PSO algorithm to determine the optimal value of the membership function corresponding to the control chart parameters. Finally, simulation findings indicated that the raised control chart outperformed others in economic and statistical standards under different positional and scale parameter changes (Amiri et al., 2023). Mao et al. (2022) studied the anti-noise effect of model identification based on the two population cooperative PSO algorithm, and the model parameters were obtained by the algorithm with the adaptive dynamic sliding window. Simulation studies have shown that in contrast to the two existing parameter identification methods, the average variance of this method was reduced by at least 35 dB, and the raised method could control the max error of state of charge estimation within 1%. Ding et al. (2021) used the extreme learning machine network optimized by PSO to build a neural network syndrome classification prediction model. The experiment outcomes denoted that its classification accuracy was 86.26%, and the classification accuracy for all syndromes was between 82.15% and 93.82%. Yu et al. (2022) and others creatively applied PSO to optimize the spiral groove shape of end milling cutter and the curvature radius of spiral groove curve. The iteration times were set to 200. In the 32nd iteration, the result arrived infinitesimal, and the final function converged to obtain the curvature radius of the milling cutter groove. The optimized eccentricity of the end milling cutter was infinitely small, which could fully utilize the vibration reduction effectiveness of the end milling cutter (Yu et al., 2022).

Barbu (2023) used SURF and HOG based features to perform color image feature extraction at each scale,

and the feature vectors were then connected into the final descriptor. A new vehicle tracking technique was proposed by utilizing the distance between these feature vectors. This method has shown good detection and tracking performance in research findings. Keyvanpour et al. (2021) constructed a image registration framework based on texture feature extraction, and used key assessment indicators to express the analysis and qualitative comparison between each method, which simplified the accurate selection of the proposed methods for the intended application. Wei & Zhang (2021) established a feature extraction network based on metric learning supervision, which could obtain the distinguishing features of products. Finally, a product image retrieval method with clustering attention was elaborated. Its performance has been verified. The research outcomes provided reference for feature extraction and retrieval in other image processing fields. Liang et al. (2022) proposed a local feature point extraction (LFPE) algorithm for depth color image registration. To evidence algorithm's accuracy and efficacy, comparisons were made with FAST, SURF, and BRISK algorithms. The experiment outcomes expressed that the accuracy of the LFPE algorithm was 1.6 times that of BRISK, 3.5 times that of FAST, and 40.1 times that of SURF. Jiang et al. (2019) proposed the gravitational particle swarm optimization algorithm, which showcases an interesting hybrid strategy and perfectly combines the collective behavior of the particle swarm algorithm with the Newton's law of gravity of the genetic algorithm. GPSOA updates the velocity of particles through the random cooperation of GSA gravity acceleration and PSO velocity. In the joint economic scheduling problem of wind, heat and electricity, the effectiveness of combining particle swarm optimization algorithm with other algorithms has been demonstrated .

He et al. (2018a) proposed a new analog circuit fault diagnosis method that utilizes features extracted from the time-frequency representation of signals and improved vector valued regularized kernel function approximation (VVRKFA) for fault diagnosis. Firstly, cross wavelet transform is used to generate the energy phase distribution of the fault signal in the time and frequency domains. Due to the high-dimensional nature of the distribution, supervised dimensionality reduction techniques such as bilateral 2D linear discriminant analysis are applied to construct a concise feature set from the distribution. Finally, use VVRKFA for fault localization. In order to improve classification performance, quantum particle swarm optimization technology is used to gradually adjust the learning parameters of the VVRKFA classifier. He et al. (2018b) proposed a new method for analog circuit fault diagnosis based on cross wavelet singular entropy feature extraction and support vector machine. Firstly, cross wavelet transform (XWT) is utilized to effectively suppress environmental noise and convert fault signals into time-frequency spectrum (TFS). Then, use a simple segmentation method to decompose the TFS into several blocks. Analyze the blocks using Singular Value Decomposition (SVD) and obtain the Tsallis entropy of each block to construct the original features. Subsequently, these features are introduced into parameter t-distribution random nearest neighbor embedding (t-SNE) for

dimensionality reduction to generate discriminative and concise fault features. Finally, the fault features are input into the SVM classifier, and the quantum particle swarm optimization algorithm is used to determine the free parameters of the SVM to locate circuit defects. The simulation results show that this method has better diagnostic performance than other existing methods. Zhang et al. (2023) proposed the Manhattan distance curve to quantify the charging voltage variation curve, and then detect and locate faulty batteries in lithium-ion battery packs. A voltage difference analysis method was proposed, which uses different criteria to determine the type of fault based on three types of fault characteristics. Based on the aging data of series lithium-ion battery packs, the effectiveness of multi fault diagnosis technology was verified through diagnostic experiments. The diagnostic experimental results show that this method can sensitively and reliably detect and isolate multiple faults, and has the advantages of low computational complexity and high accuracy.

In summary, many scholars have conducted extensive research on PSO algorithms and feature extraction algorithms, and applied the proposed methods to various fields, achieving certain results. In most methods, although the algorithm has a simple structure, there is still space for improvement in classification accuracy and registration rate, and the running time of the model is also relatively long. Therefore, it is a novel way to combine the swarm intelligence algorithm with the PSO model, and introduce adaptive inertia weight (IW) and chaos model to improve the PSO. The research aims to improve the recognition performance of CDP images.

MATERIAL AND METHODS

PSO has certain feasibility in optimization problems, but the initial population is uncertain, and it is prone to drop into local optimum in the iteration. Therefore, some scholars use the randomness and ergodicity of chaos theory to propose a chaotic particle swarm optimization (CPSO) (Kotla & Yarlagadda, 2021; Ho et al., 2021; Nabavi et al., 2022). CPSO has improved the problem of PSO in practical applications, but the assignment of IWs requires manual adjustment, which has a significant impact. Therefore, an ACPSO algorithm is proposed to address this issue. Finally, SVM is used to classify the model results (Malik et al., 2021; Raj et al., 2022). There are three main reasons for choosing the ACPSO-SVM algorithm in crop disease and pest identification research: firstly, the algorithm has efficient parameter optimization. The ACPSO algorithm combines particle swarm optimization and individual learning strategies, which can effectively overcome the problem of conventional PSO algorithms falling into local optima during parameter search. Through adaptive and comprehensive optimization strategies, the ACPSO-SVM algorithm can provide more efficient parameter optimization capabilities, thereby improving the performance and accuracy of classification models. Secondly, the algorithm has good robustness and

generalization ability. Support Vector Machine (SVM) is a machine learning based classification method with strong robustness and generalization ability, which can maintain good predictive performance even when facing a small number of training samples or noisy data. The ACPSO SVM algorithm combines the advantages of SVM and further improves the robustness and generalization ability of the classification model through the ACPSO algorithm, making it more adaptable in crop pest and disease identification. Thirdly, the algorithm has the ability to process high-dimensional feature spaces. In crop pest and disease recognition, the feature dimension is usually higher because multiple features such as color, texture, morphology, etc. need to be considered. The SVM algorithm transforms low dimensional feature spaces into higher dimensional feature spaces through kernel function mapping, thereby better processing high-dimensional data. The ACPSO-SVM algorithm can effectively classify and accurately identify crop diseases and pests in high-dimensional feature spaces.

Construction of recognition model based on ACPSO-SVM algorithm

The chaotic system used by CPSO is a logistic mapping, and its expression is shown in formula (1).

$$X_{n+1} = X_n * \mu * (1 - X_n) \quad (1)$$

In formula (1), X_n means the Logistic mapping result; μ denotes the control parameter. When the Logistic model is in a totally chaotic status, the value of the control parameter is 4. It assumes that the model undergoes a certain number of iterations, the resulting chaotic vector is denoted as β_{ik} , where i indicates the dimension of the chaotic vector and k expressed the iteration times of the model. It maps the obtained chaotic operation vector between $[0,1]$ as X_k , and records the chaotic vector after implementing uncertainty mixing as X_{k+1} . The expression is shown in formula (2).

$$X_{k+1} = (1 - \alpha)X_k + \alpha\beta_k \quad (2)$$

In formula (2), α refers to the chaotic vector equilibrium coefficient. If the fitness value obtained by particle iteration is denoted as f , then f_g denotes the optimal particle fitness value, the average fitness value is denoted as f_{avg} , and the average value superior to f_{avg} is denoted as f'_{avg} . Then the adaptive adjustment strategy needs to meet the following three constraints: First, if f is greater than f'_{avg} , f can be regarded as the global optimum. Setting the IW value of the model to a smaller value can speed up the global optimum Rate of convergence speed. The IW is recorded as ω , and its expression is shown in formula (3).

$$\omega = \omega - (\omega - \omega_{\min}) \times \frac{|f_i - f'_{avg}|}{f_g - f'_{avg}} \quad (3)$$

In formula (3), the minimum value of IW is 0.5. Secondly, when the particle is an ordinary particle in the population, i.e. $f_{avg} < f_i < f'_{avg}$, the expression for IW is expressed in formula (4).

$$\omega = \omega_{\min} + (\omega_{\max} - \omega_{\min}) \times \frac{1 + \cos(k-1)\pi / (K-1)}{2} \quad (4)$$

In formula (4), K refers to the max iteration times of the model. Thirdly, when the particle is the weaker particle in the population, i.e. $f_i < f'_{avg}$, the expression of IW is indicated in formula (5).

$$\omega = 1.5 - \frac{1}{1 + a_1 \times \exp(-a_2 \times (f_{avg} - f'_{avg}))} \quad (5)$$

In formula (5), a_1 and a_2 are constants with values greater than 1. Whether the particle swarm undergoes premature convergence can be determined by the value of $f_{avg} - f'_{avg}$. The smaller the value, the earlier the particle swarm converges; If the particle swarm approaches the local optimal range, the update speed of the model will become slower until the end. In the recognition of CDP, color, texture, shape, and local features need to be recognized, and finally classified using SVM. The process framework based on ACPSO-SVM is shown in Figure 1.

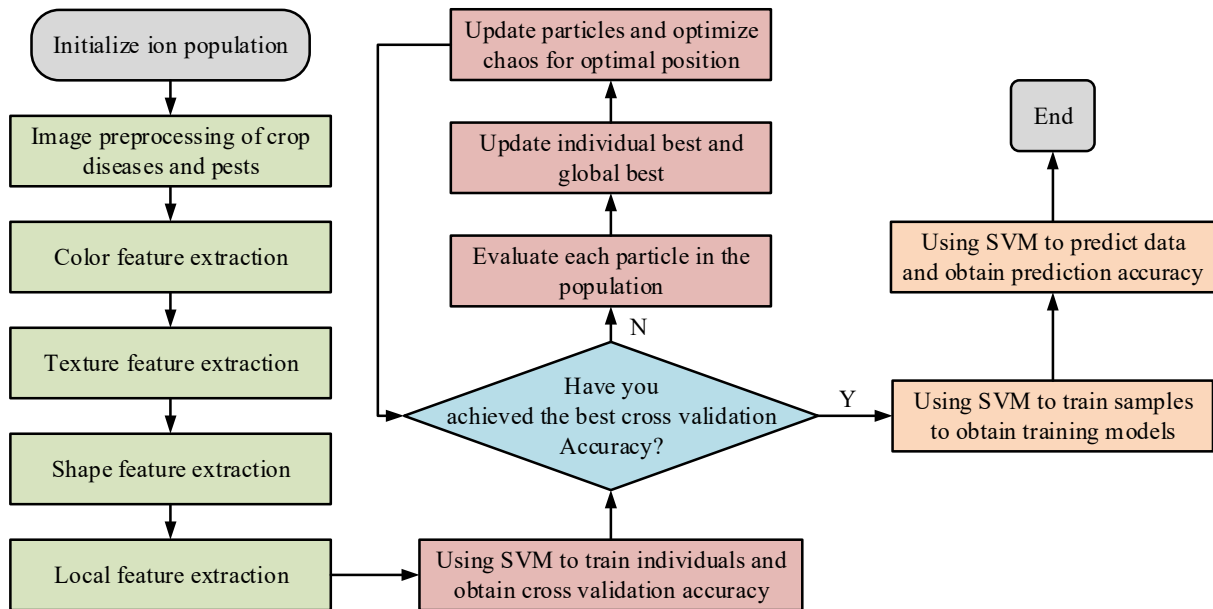


FIGURE 1. Process framework diagram based on ACPSO-SVM.

Color and texture feature extraction based on ACPSO-SVM model

In the ACPS-SVM model constructed through research, multiple feature fusion methods are used to process CDP images. In color feature extraction, a color feature fusion algorithm using a new color space and color moments is studied. This algorithm utilizes the low dimensionality, rotation, and scaling invariance of color moments to perform Red, Green, and Blue (RGB) components on crop images. The feature extraction of color moments does not require the quantification of features, so the three color components of color moments each have three lower order moments, totaling nine components. The first moment (mean) generally represents the average value of colors, as shown in formula (6).

$$\tau_i = \frac{\sum_{j=1}^N p_{i,j}}{N} \quad (6)$$

In formula (6), τ refers to the mean color; $p_{i,j}$ means the probability of color components appearing in pixels; N denotes the amount of pixels in the image. The second order moment (Variance) generally represents the variance of the color component, and its expression is shown in formula (7).

$$\sigma_i = \sqrt{\frac{1}{N} \sum_{j=1}^N (p_{i,j} - \tau_i)^2} \quad (7)$$

In formula (7), σ_i is the variance of the color component. The third moment (Skewness) generally represents the covariance of the color component, and its expression is denoted in formula (8).

$$s_i = \sqrt[3]{\frac{1}{N} \sum_{j=1}^N (p_{i,j} - \tau_i)^3} \quad (8)$$

In formula (8), s_i expressed a 9D histogram vector composed of the first three color moments of the R, G, and B components of the image, and the color features of the image are represented as expressed in formula (9).

$$F_{color} = [\tau_R, \sigma_R, s_R, \tau_G, \sigma_G, s_G, \tau_B, \sigma_B, s_B] \quad (9)$$

It converts the RGB color space into a new color space, represented by O_1 , O_2 , and O_3 , respectively. In crop images, color features cannot fully describe the image, so texture features are also added to the feature extraction. In which, a method combining gray level co-occurrence matrix (GLCM) with local binary pattern (LBP) is put forward (Bazikar et al., 2022; Rehman et al., 2022). GLCM is a second-order combined conditional probability density function of an image, which describes the relative frequency of different gray level pixels appearing again in the window. GLCM performs statistics on pixel coordinates, and the probability of relative frequency can be calculated using formula (10).

$$p(m, n, d, \theta) = \# \left\{ \begin{array}{l} (x, y), (x + \Delta x, y + \Delta y) \in D \\ f(x, y) = m \\ f(x + \Delta x, y + \Delta y) = n \end{array} \right\} \quad (10)$$

In formula (10), m and n represent different gray levels; d refers to the distance between gray levels; θ means the angle; $p(m, n, d, \theta)$ expressed the probability of m and n appearing along θ in d ; $\#\{\Omega\}$ stands for the amount of elements in the set; $(x + \Delta x, y + \Delta y)$ represents the pixel coordinates after Pixel shift; D means the range of the image. From formula (10), if the distance and angle values of different grayscale pixels are different, the number of co-occurrence matrices will vary, and the spatial information of pixels will also change. The calculation diagram of the GLCM is shown in Figure 2.

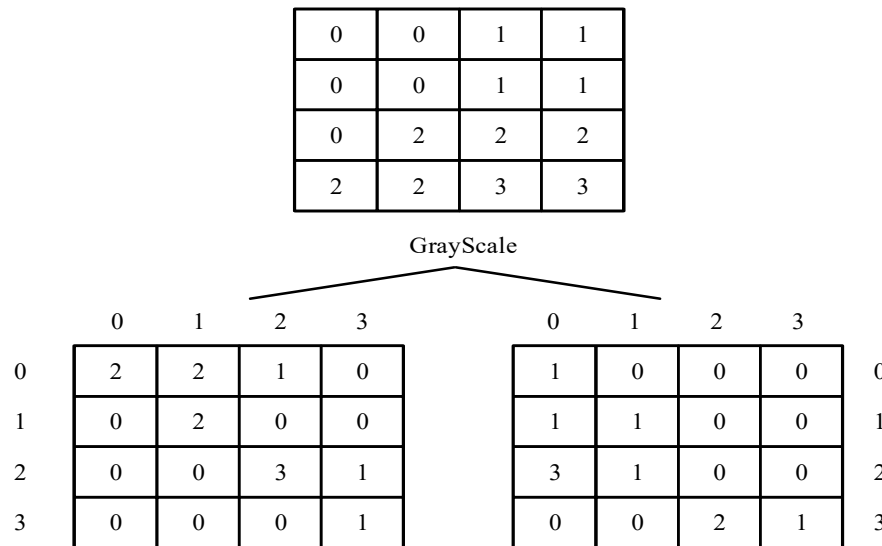


FIGURE 2. Calculation diagram of GLCM

Figure 2 calculates the image size of 4 * 4 with a gray level value of 0-3 and a distance of 1 to obtain two different GLCMs. The texture feature vectors based on the GLCM method have four representations: entropy, energy, moment of inertia, and correlation. Among them, entropy is a random variable containing texture information in the image, and its calculation method is denoted in formula (11).

$$ENT = -\sum_{m,n} \{p(m, n, d, \theta)\} \log \{p(m, n, d, \theta)\} \quad (11)$$

In formula (11), ENT expresses entropy value, and its value size reflects the randomness of pixel value distribution. Energy is a measure of the stability of gray level changes in texture features. By calculating the sum of squares of each value in GLCM, it can reflect the texture thickness and uniform distribution of gray level. Its calculation is shown in formula (12).

$$ENR = \sum_{m,n} \{p(m, n, d, \theta)\}^2 \quad (12)$$

In formula (12), ENR refers to the energy value, and the larger its value, the more stable the image texture rules are. The moment of inertia measures the differential changes between pixels within a local range, reflecting the clarity and depth of the texture. Its value is calculated as shown in formula (13).

$$CON = \sum_m \sum_n (m - n)^2 p(m, n, d, \theta) \quad (13)$$

In formula (13), CON indicate the moment of inertia, and its value represents the clarity of the image. The correlation quantity reflects the local grayscale correlation and measures the similarity of each row or column in GLCM. Its calculation is denoted in formula (14).

$$COR = \frac{\sum_{m,n} (m - \tau_x)(n - \tau_y) p(m, n, d, \theta)}{\sigma_x \sigma_y} \quad (14)$$

In formula (14), *COR* stands for the correlation quantity. The expression of LBP fused with GLCM is shown in formula (15).

$$\left\{ \begin{aligned} LBP_{P,R}^{riu2} &= \begin{cases} \sum_{p=0}^{p-1} s(g_p - g_c) 2^p, T(LBP(P, R) \leq 2) \\ p + 1, other \end{cases} \\ U(LBP(P, R)) &= |s(g_{p-1} - g_c) - s(g_0 - g_c)| + \sum_{i=1}^{p-1} |s(g_i - g_c) - s(g_{i-1} - g_c)| \\ s(x) &= \begin{cases} 1, x \geq 0 \\ 0, x < 0 \end{cases} \end{aligned} \right. \quad (15)$$

In formula (15), *R* expresses the radius defined by LBP; *p* refers to pixels with a circular area; *g_c* means the grayscale value of the center point; *g_p* represents the grayscale value in the circular area; *T(LBP(P, R))* refers to the uniformity index of the LBP operator.

Shape and local feature extraction based on ACP SO-SVM model

In the research of shape feature extraction, the Hu moment invariant method is adopted. The moment invariant has translation, scale and Rotational invariance, which is a statistical feature. It assumes that *f(x, y)* is two-dimensional continuous, then in the integral region, the matrix is expressed in formula (16).

$$m_{wQ} = \int \int x^w x^Q f(x, y) dx dy, W, Q = 0, 1, 2... \quad (16)$$

In formula (16), *m_{wQ}* means the *Q + W* order matrix, *Q* represents the number of rows in the matrix, *W* represents the number of columns in the matrix. If the *f(x, y)* function of a digital image is continuous and segmented, and there are non zero values in the two-dimensional memory, then the moments of each order can be proven. The calculation of centre-to-centre distance is shown in Formula (17).

$$U_{wQ} = \int \int (x - x_c)^w (y - y_c)^Q f(x, y) dx dy \quad (17)$$

In formula (17), *U* stands for the centre-to-centre distance and its normalized form is shown in formula (18).

$$\left\{ \begin{aligned} \eta_{QW} &= U_{QW} / U_{00}^\rho \\ \rho &= (Q + W) / 2 + 1 \end{aligned} \right. \quad (18)$$

In formula (18), *η* denotes the normalized value and *ρ* refers to the average order of centre-to-centre

distance. The research adopts the improved speed up robust feature (SURF) algorithm for local feature extraction, which is particularly important in key point detection, locating key point directions, and feature vector construction (Saidi et al., 2021). It assumes that there is a point in the image, the Hessian matrix with scale *σ* is shown in formula (19).

$$H(x, \sigma) = \begin{bmatrix} E_{xx}(x, \sigma) & E_{xy}(x, \sigma) \\ E_{xy}(x, \sigma) & E_{yy}(x, \sigma) \end{bmatrix} \quad (19)$$

In formula (19), *E_{xx}(x, σ)* denotes pixel values and *H(x, σ)* expressed the Hessian matrix. The critical point is the extreme value of the determinant of the Hessian matrix, and its determination method is indicated in formula (20).

$$\det(H_{approx}) \approx E_{xx} E_{yy} - (w E_{xy})^2 \quad (20)$$

In formula (20), *w* stand for the compensation parameter, and in general, its value is 0.9. The determination of the direction of locating key points is based on the Haar wavelet basic function, as denoted in formula (21).

$$\varphi(x) = \begin{cases} 1 & x \in [0, \frac{1}{2}) \\ -1 & x \in [\frac{1}{2}, 1] \end{cases} \quad (21)$$

In formula (21), *φ(x)* denotes the Haar wavelet fundamental function. The calculated wavelet response value and the gap between the feature points and the center of the circle are assigned weights, so that the weight obtained by the key points closer to the center of the circle is greater. To obtain the positioning direction of key points, it is necessary to construct a feature vector, which can operate on the key points and obtain all main directions, as shown in Figure 3.

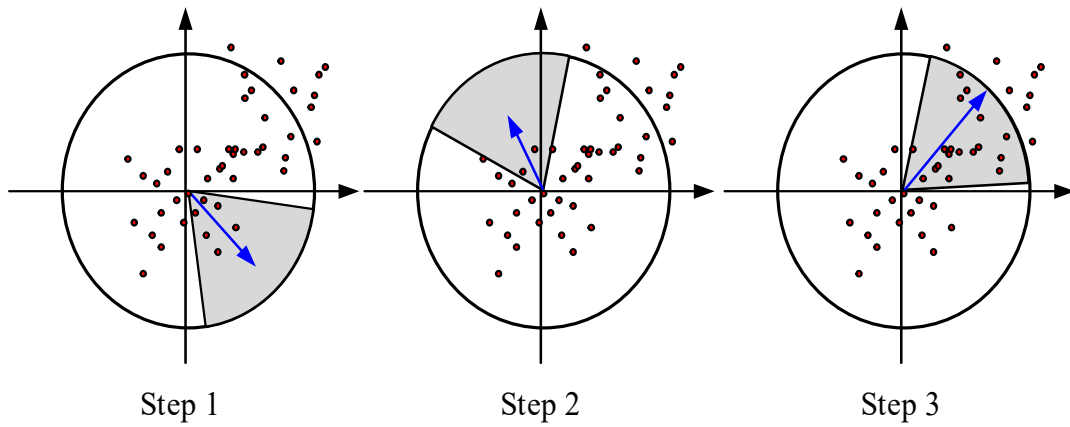


FIGURE 3. Schematic diagram for determining the main direction of key points

Figure 3 shows the construction of feature vectors. The method first involves constructing a 60 degree sector, traversing the circle at certain intervals, and adding the weights within each sector region to obtain a new vector. For each interval moved, a vector can be obtained within the sector area, and the main direction to be determined is the direction of the longest vector among all feature vectors. By operating on each key point using this method, all main directions can be determined. After determining the main direction of key points, feature vectors need to be constructed. By determining the Haar wavelet response values in the horizontal and vertical directions, a four-dimensional vector representation can

be obtained as shown in formula (22).

$$vector = (\sum dx, \sum dy, \sum |dx|, \sum |dy|) \tag{22}$$

In formula (22), dx and dy express the horizontal and the vertical Haar wavelet responses, respectively. In the above construction model, the features to be detected have a high sensitivity to image transformation. Therefore, the study used Box Fileters' counterclockwise rotation as an alternative, and the improved SUURF box filter rotation method is indicated in Figure 4.

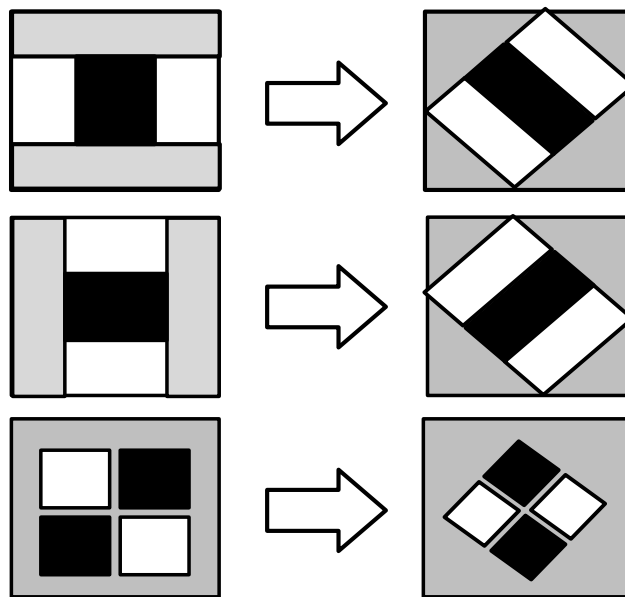


FIGURE 4. Schematic diagram of improved SUURF box filter rotation.

The detection operator based on the Hessian matrix exhibits the weakest repeatability when the image is rotated at an odd multiple angle of 45°. Therefore, when Box Fileters rotate at the same angle, the response results will be more stable for image rotation and other transformations. Box Fileters that rotate 45°

counterclockwise can effectively combine with the original filter and algorithm. When the SURF filter is rotated 45°, the four array search speed advantage of each filter can still be maintained. The four array indexes used to calculate the sum of pixels in the rotated Box Fileters area are shown in Figure 5.

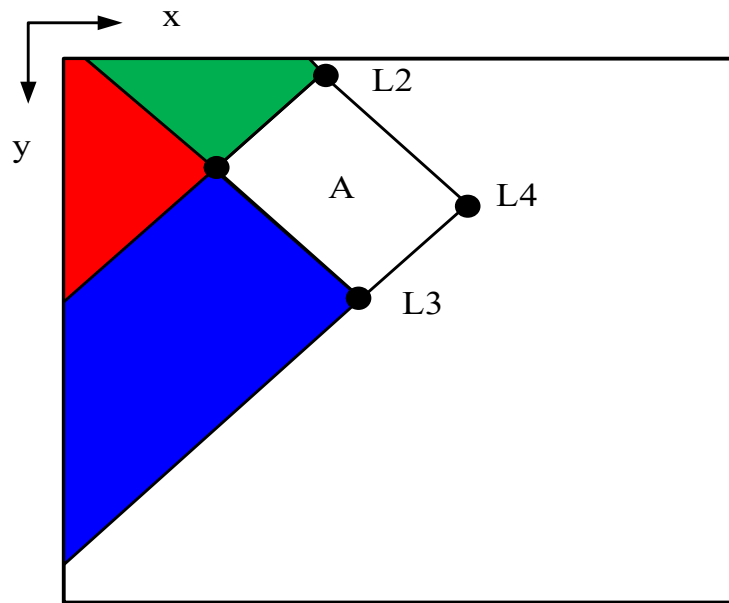


FIGURE 5. Pixel sum based on rotation region.

The calculation method of pixel sum in Figure 6 can be illustrated by formula (23).

$$A = L_4 + L_1 - L_2 - L_3 \quad (23)$$

In formula (23), L denotes the pixel value; A means the sum of pixel values. The size of the Hessian determinant threshold represents the strength of the features of the corresponding position in the image. In SURF algorithm, the Hessian determinant threshold is used as a criterion to screen feature points. Further research is conducted on the complexity analysis of the constructed ACP SO-SVM model. Assuming that the algorithm uses N_{iter} to represent the number of iterations during the calculation process, the number of particle swarm populations is represented by N , and the dimensions of particles are represented by $2M$. The computational complexity of converting particle matrices into adaptive chaotic matrices is $O(N(2M))$; The computational complexity of obtaining fitness values based on adaptive chaos is $O(N(2M))$; The computational complexity of particle population evolution is $O(2N(2M))$. Therefore, the total complexity of the proposed model is shown in formula (24).

$$O(N_{iter}(N + N + 2N(2M))) = O(8N_{iter}NM) \quad (24)$$

In formula (24), the computational complexity of the algorithm is linear, therefore the overall computational complexity is relatively low.

RESULTS AND DISCUSSION

To study the methods of crop pest classification and recognition, the AI Challenger 2018 dataset was selected for training and performance testing of the constructed model. It is a dataset of crop leaf images, with a total of 50000 annotated images. Research and study 5000 images as the training set of the model, and select 1000 images as the test set of the model. The images mainly contain three diseases, namely, two spore leaf spot disease, algae spot disease, and gray spot disease. The simulation experiment was conducted using MATLAB 2013. The hardware configuration of the experiment is as follows: the processor is Inter Core i7-4710MQ, the operating system is Windows 7, and the memory size is 4GB. Firstly, training experiments were conducted to train the model and study its recognition and classification performance; Then, the model is used for practical testing and its performance is verified through actual application and comparison with other models.

Analysis of model performance based on ACP SO-SVM

The experiment selected a testing function to test the effect of the selected algorithm, and compared and analyzed several similar algorithms. Similar algorithms include CPSO, PSO, binary chaos particle swarm optimization (BCPSO), and linear decreasing strategy particle swarm optimization (LDS-PSO). Meanwhile, the parameters of the algorithm were set to the optimal values, and all methods were run 30 times. The variance and mean best fitness values of the algorithm are shown in Figure 6.

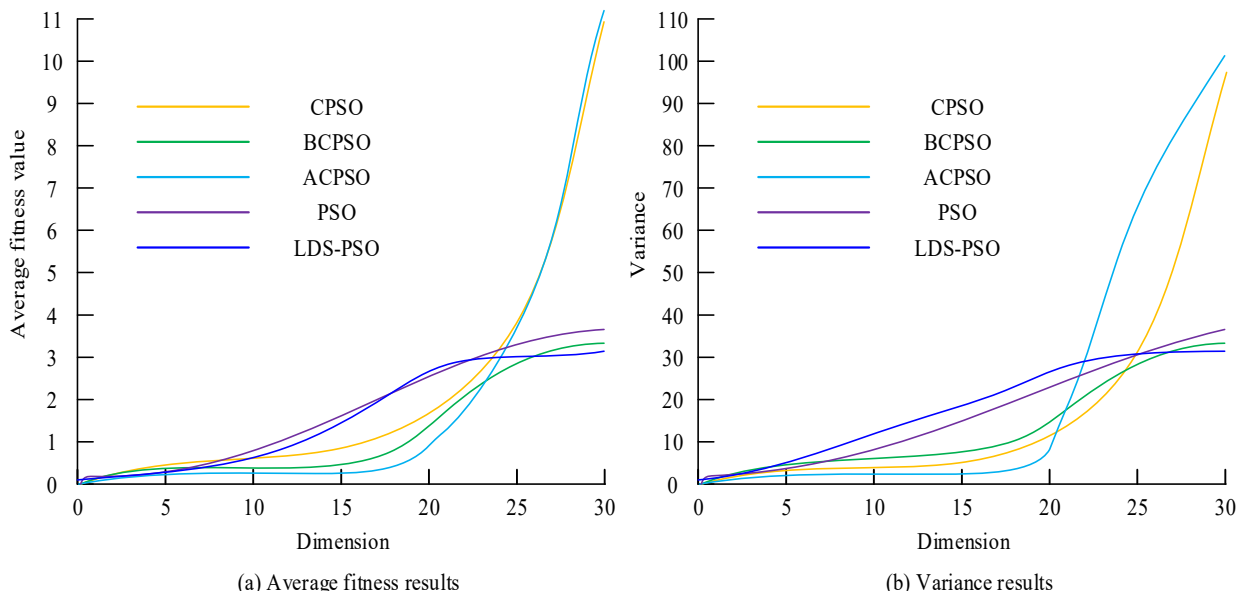


FIGURE 6. Average fitness values and variance results of different algorithms.

In Figure 6, for the test function, compared with 5 PSO algorithms in 10, 20 and 30 dimensions, the average fitness value of ACP SO was 0.2677, 1.0028 and 10.3474, respectively, and the variance of ACP SO was 2.6771, 8.5019 and 71.3189, respectively. Its fitness value and variance performance were the best. In summary, among various dimensional functions, the ACP SO algorithm had

certain advantages and good optimization performance. The study selected 90 experimental samples, which were three pests and diseases of Guiyuan, namely gray spot disease, shell spore leaf spot disease, and algal spot disease. The color feature extraction method of the model was tested using the above samples, and the results are shown in Figure 7.

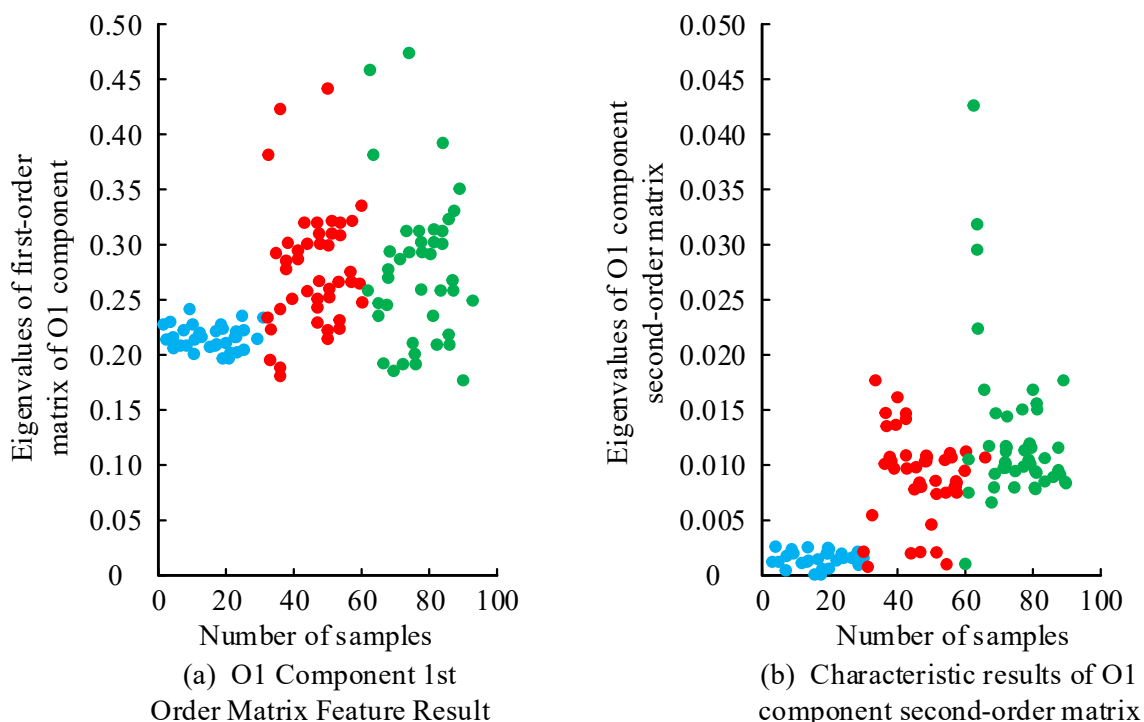


FIGURE 7. Distinguishing results of fusion of new color space and color moment features

Figure 7 shows the characteristic values of the two stages of the new color component. The distribution results of Figure 7 (a) indicated that the three pests and diseases have been effectively distinguished, but there were still overlapping parts of pests and diseases. Moreover, the distribution of fusarium oxysporum leaf spot disease and algae spot disease was relatively scattered in the first order moment. The distribution results of Figure 7 (b) expressed

that the distribution of gray spot disease was relatively dense, the distribution of binary leaf spot disease was relatively scattered, and the distribution effect of algal spot disease was very scattered, and there were still overlapping parts in the distribution. The specific fusion parameter values for the new color space and color moment features are displayed in Table 1.

TABLE 1 Parameter values for fusion of new color space and color moment features.

	Gray leaf spot	Ascochyta leaf spot	Algal spot disease
O ₁ component 1st moment	0.21688	0.27976	0.28598
O ₁ component 2nd moment	0.00132	0.00810	0.01978
O ₁ component 3rd moment	0.00015	0.00270	0.01174
O ₂ component 1st moment	0.36380	0.42133	0.57059
O ₂ component 2nd moment	0.01840	0.01383	0.00031
O ₂ component 3rd moment	0.00365	0.01095	-0.00051
O ₃ component 1st moment	0.51669	0.54441	0.50647
O ₃ component 2nd moment	0.02020	0.05118	0.01875
O ₃ component 3rd moment	0.00146	-0.00429	0.00135

In the results of Table 1, the fusion parameter values of the new color space and color moment features had different values in different components and stages. However, in the first moment of the O₁ component, the values of shell spore leaf spot disease and algal spot disease were relatively similar, with values of 0.27976 and 0.28598, respectively; In the second moment of O₂ component, the values of gray spot disease and shell spore leaf spot disease were relatively similar, with values of 0.01840 and 0.01383, respectively; In the third moment of

O₃ component, the values of gray spot disease and algal spot disease were relatively similar, with values of 0.00146 and 0.00135, respectively. The outcomes denoted that there was a phenomenon of overlap in color feature extraction, which affected discrimination. Therefore, it was necessary to comprehensively consider other feature extraction methods for feature extraction. The research combined texture feature extraction and the recognition accuracy results in the test set are shown in Figure 8.

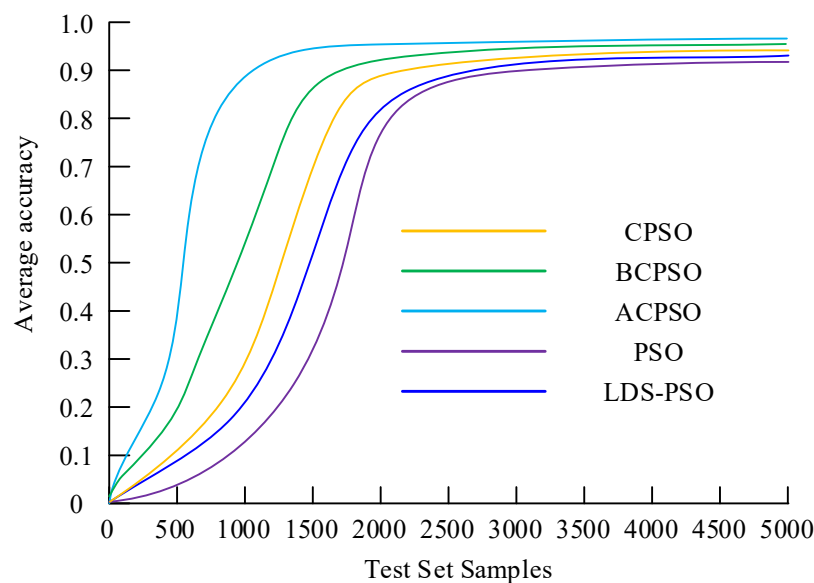


FIGURE 8. Recognition accuracy results in the test set.

In Figure 8, the recognition accuracy of all five algorithms increased with the increase of sample size. Among them, the average accuracy of PSO algorithm was 91.60%. Compared with other algorithms, PSO algorithm had the lowest accuracy and the slowest rate of convergence; The average accuracy of the ACPSO algorithm was 95.08%, and convergence occurred earliest. The findings denoted that the raised method had higher recognition accuracy and faster rate of convergence.

Analysis of the effectiveness of the model in practical

application of CDP

The ACPSO model has shown good performance after being trained on a test set. Therefore, the study would analyze the practical application of this model. The experiment analyzed 200 images of longan pests and diseases, and performed a series of physical transformations on the images, including translation, rotation, and scale transformation. Finally, the model calculated the image features as expressed in Table 2.

TABLE 2 Calculation results of invariant moment shape features.

	Original drawing	Rotate	Reduce	Amplify
Invariant moment	7.4295×10^{-4}	7.4295×10^{-4}	7.4289×10^{-4}	7.4302×10^{-4}
Number of lesions	7.8724×10^{-8}	7.8724×10^{-8}	7.9734×10^{-8}	7.4141×10^{-4}
Ratio of area to number of lesions	2.0114×10^3	5.6146×10^1	1.7963×10^2	2.4301×10^2
Area	1.1771×10^1	4.2786×10^2	9.6764×10^0	1.4224×10^1
Perimeter	5.9027×10^8	1.3064×10^9	4.9455×10^9	7.3312×10^9
Tightness consistency	7.2049×10^3	-2.2247×10^6	6.4930×10^3	9.3367×10^3
Error	-1.4999×10^8	1.2785×10^8	-1.2486×10^8	-2.2062×10^8

Note: "*" represents multiplication operation

In Table 2, after translation, rotation, and scale transformation of the original image, the consistency of invariant moments, number of lesions, area to number of lesions ratio, area, perimeter, and compactness was good, but there were still some small errors, which were mainly caused by the digitization of the data itself. The outcomes indicated that the shape features of the image became

stable after invariant moments, which also matched the shape features and could clearly represent the shape content of the image. To verify the effectiveness of this method, relevant tests were conducted on the impact of the improved operator on the efficacy of angle transformation registration. The test outcomes are indicated in Figure 9.

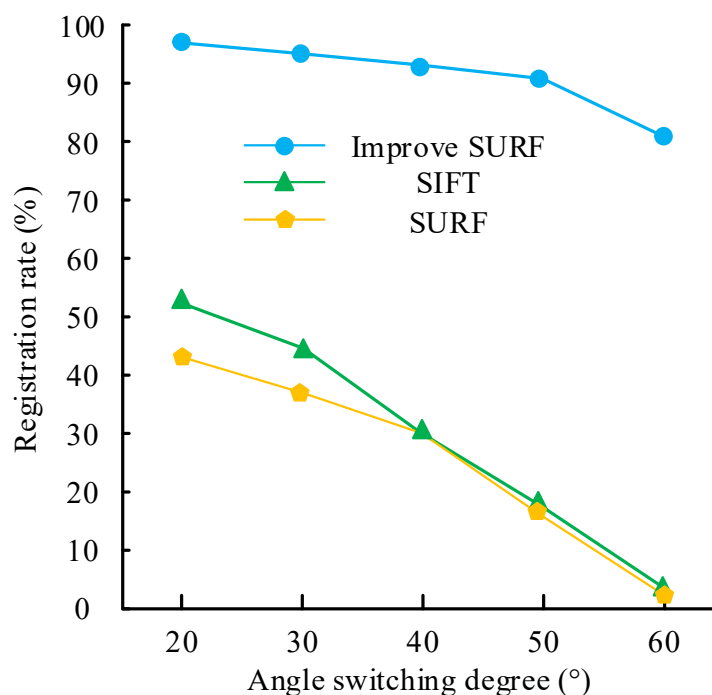


FIGURE 9. Registration results of different operators in visual transformation

In Figure 9, there were three operators for registration comparison, including the scale invariant feature transform (SIFT), SURF and the SURF that has been studied and improved. The visual transformation was from 20° to 60°, with the registration rate of SURF algorithm gradually decreasing from 41.3% to 7.65%; The registration rate of the SIFT algorithm gradually decreased from 52.1%

to 7.70%; The improved algorithm gradually decreased from 98.5% to 84%. The experiment findings denoted that the improved algorithm had high registration rate and good anti-interference performance in visual transformation. The experiment was conducted using images of longan pests and diseases, and 200 sets of longan pest and disease images were identified. The results are shown in Figure 10.

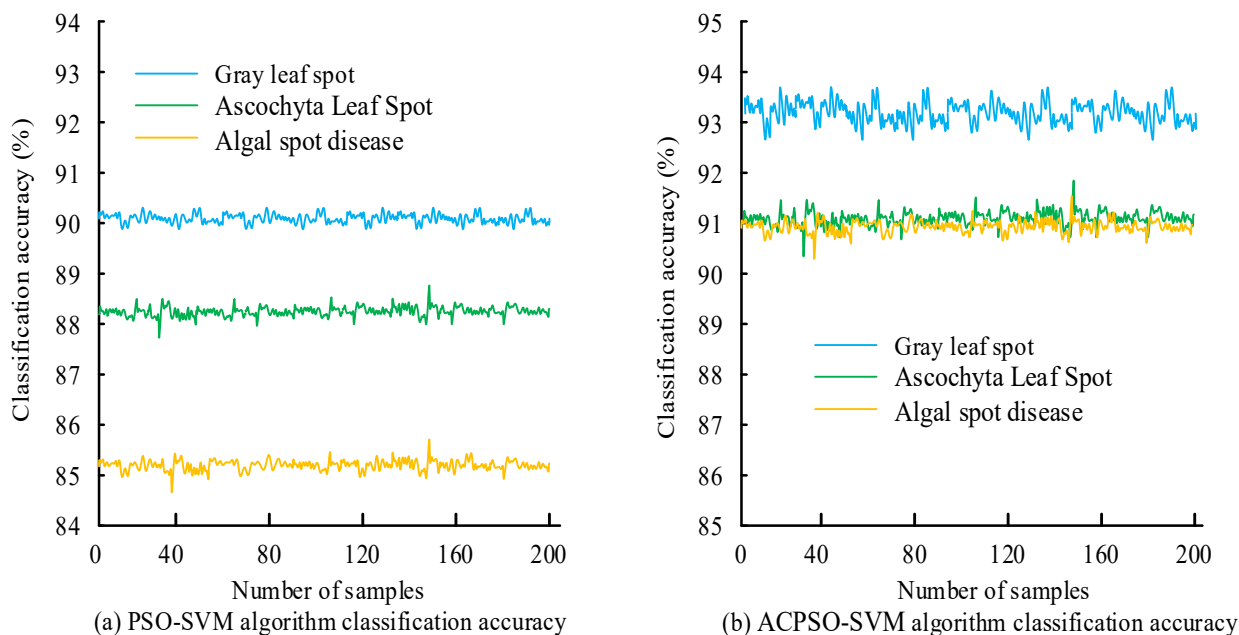


FIGURE 10. Classification results of diseases and pests in longan using different algorithms.

Figure 10 expresses the comparison results of classification accuracy. The PSO-SVM algorithm was utilized for comparative experiments. The recognition accuracy of PSO-SVM for gray spot disease was 90.39%, and the recognition accuracy of ACP SO-SVM was 93.29%; The recognition accuracy of fusarium oxysporum leaf spot disease was 88.44%, and the recognition accuracy of ACP SO-SVM was 91.11%; The recognition accuracy of algae spot disease was 85.39%,

and the recognition accuracy of ACP SO-SVM was 90.94%; The average classification accuracy of PSO-SVM was 88.07%, while that of ACP SO-SVM was 91.78%. The experimental findings indicated that the ACP SO-SVM model proposed in the study had good recognition performance in CDP. In order to further verify the performance of the proposed model, other algorithms are also used for actual comparative analysis, and the results are shown in Table 3.

TABLE 3. Classification accuracy and running time of pests and diseases using different classification methods.

Types of pests and diseases	Classification accuracy(%)				Run time(s)			
	CPSO	APSO	PSO-SVM	ACP SO-SVM	CPSO	APSO	PSO-SVM	ACP SO-SVM
Gray spot disease	87.94	88.07	90.28	93.18	88.071	90.211	92.592	87.098
Ascochyta Leaf Spot	85.99	86.12	88.33	91.00	95.665	97.805	100.186	84.061
Algal spot disease	82.94	83.07	85.28	90.83	91.805	93.945	96.326	85.032
Average value	85.62	85.75	87.96	91.67	91.847	93.987	96.368	86.697

In Table 3, the classification accuracy of the ACP SO-SVM method was improved to 93.18%, 91.00%, and 90.83%, respectively, based on 87.94%, 85.99%, and 82.94%, respectively. This indicates that the ACP SO-SVM method has better performance and accuracy in identifying these pests and diseases. The PSO-SVM and ACP SO-SVM methods have relatively longer runtime, while the CPSO and APSO methods have shorter runtime. Therefore, in practical applications, it is necessary to comprehensively consider the trade-off between classification accuracy and runtime. According to the data, ACP SO-SVM performs best in classification accuracy and average value, indicating that this method has high stability and accuracy in dealing with the identification problems of these pests and diseases. In summary, the ACP SO-SVM method has shown better performance and accuracy in the classification and recognition of these pests and diseases.

CONCLUSIONS

The research focused on the recognition and classification of CDP images. In the framework of ACP SO algorithm, swarm intelligence algorithm was used to optimize all aspects of image classification and recognition, and then a CDP image recognition model based on ACP SO-SVM was proposed. This model optimized color, texture, shape and local feature extractions in the image processing stage. Based on CPSO, adaptive IW adjustment was introduced, and finally, SVM was combined for image classification. The performance analysis of the ACP SO SVM model was conducted through comparative experiments, and the outcomes expressed that the average fitness of the ACP SO SVM model in 30 dimensional images was 10.3474, with a variance of 71.3189; The average correct rate in the test set was 95.08%, and it had a fast rate of convergence; The average classification

accuracy in practical applications reached 91.78%. The outcomes indicated that the algorithm put forward in the study was feasible and had good results in identifying CDP. However, there were still shortcomings in the research. The study only focused on the leaf diseases and pests of crops, without considering the symptoms of diseases and pests such as stems and fruits. To raise the accuracy of recognition and classification and the practicality of research, subsequent research can comprehensively consider the feature information of different parts and conduct comprehensive classification and recognition research on these pest and disease images.

ACKNOWLEDGEMENTS

This research was supported by the fundamental research project (General Project) of Liaoning provincial department of education 2022 (LJKMZ20221691), Liaoning Institute of Science and Technology Doctoral Start-up Fund 2023 (2307B06), Pioneer Research Team of Liaoning Institute of Science and Technology "Technology and Application of Big Data and Intelligent information Processing" (XPT202306).

REFERENCES

- Amiri A, Salmasnia A, Zarifi M, Maleki MR (2023) Adaptive shewhart control charts under fuzzy parameters with tuned particle swarm optimization algorithm. *Journal of Industrial Integration and Management* 08(02):241-276. <http://doi.org/10.1142/S2424862221500226>
- Barbu T (2023) Deep learning-based multiple moving vehicle detection and tracking using a nonlinear fourth-order reaction-diffusion based multi-scale video object analysis. *Discrete and Continuous Dynamical Systems-S* 16(1): 16-32. <http://doi.org/10.3934/dcdss.2022083>
- Bazikar F, Ketabchi S, Moosaei H (2022) Smooth augmented lagrangian method for twin bounded support vector machine. *Numerical Algebra, Control and Optimization* 12(4): 659-678. <http://doi.org/10.3934/naco.2021027>
- Dagal I, Akn B, Akboy E (2022) Improved salp swarm algorithm based on particle swarm optimization for maximum power point tracking of optimal photovoltaic systems. *International journal of energy research* 46(7): 8742-8759. <http://doi.org/10.1002/er.7753>
- Ding L, Zhang XY, Wu DY, Liu ML (2021) Application of an extreme learning machine network with particle swarm optimization in syndrome classification of primary liver cancer. *Journal of Integrative Medicine* 19(2):395-407. <http://doi.org/10.1016/j.joim.2021.08.001>
- Guo Y, Mustafaoglu Z, Koundal D (2022) Spam detection using bidirectional transformers and machine learning classifier algorithms. *Journal of Computational and Cognitive Engineering* 2(1): 5-9. <http://doi.org/10.47852/bonviewJCCE2202192>
- Ho SD, Palacky P, Kuchar M, Brandstetter P, Tran CD (2021) Particle swarm optimization-based stator resistance observer for speed sensor less induction motor drive. *International Journal of Electrical and Computer Engineering* 11(1):815-826. <http://doi.org/10.11591/ijece.v11i1.pp815-826>
- He W, He Y, Luo Q, Zhang C (2018a) Fault diagnosis for analog circuits utilizing time-frequency features and improved VVRKFA. *Measurement Science & Technology*, 29(4): 045004. <http://doi.org/10.1088/1361-6501/aaa33a>
- He W, He Y, Li B, Zhang C (2018b) Analog circuit fault diagnosis via joint cross-wavelet singular entropy and parametric t-SNE. *Entropy* 20(8):604-604. <http://doi.org/10.3390/e20080604>
- Jiang S, Zhang C, Wu W, Chen S (2019) Combined Economic and emission dispatch problem of wind-thermal power system using gravitational particle swarm optimization algorithm. *Mathematical Problems in Engineering* (2):5679361. <http://doi.org/10.1155/2019/5679361>
- Keyvanpour MR, Vahidian S, Mirzakhani Z (2021) An analytical review of texture feature extraction approaches. *International Journal of Computer Applications in Technology* 65(2): 118-133. <http://doi.org/10.1504/IJCAT.2021.114990>
- Kotla RW, Yarlagaadda SR (2021) Comparative analysis of photovoltaic generating systems using particle swarm optimization and cuckoo search algorithms under partial shading conditions. *Journal Européen des Systèmes Automatisés* 54(1):27-33. <http://doi.org/10.18280/jesa.540104>
- Liang J, Xiao K, Gao G (2022) A depth-colour image registration method based on local feature point extraction. *Biosystems Engineering* 219: 268-280. <https://doi.org/10.1016/j.biosystemseng.2022.05.008>
- Malik G, Upadhyaya S, Sharma R (2021) Particle swarm optimization and maximum entropy results for mx/g/1 retrial g-queue with delayed repair. *International Journal of Mathematical, Engineering and Management Sciences* 6(2):541-563. <https://doi.org/10.33889/IJMEMS.2021.6.2.033>
- Mao L, Zhao J, Zhu Y, Chen J (2022) A noise-immune model identification method for lithium-ion battery using two-swarm cooperative particle swarm optimization algorithm based on adaptive dynamic sliding window. *International Journal of Energy Research* 46(3): 3512-3528. <https://doi.org/10.1002/er.7401>
- Nabavi SR, Eraghi NO, Torkestani JA (2021) Wireless sensor networks routing using clustering based on multi-objective particle swarm optimization algorithm. *Journal of Intelligent Procedures in Electrical Technology (JIPET)* 12(47): 49-67. <https://dorl.net/dor/20.1001.1.23223871.1400.12.3.3.3>
- Qteat H, Awad M (2021) Using hybrid model of particle swarm optimization and multi-layer perceptron neural networks for classification of diabetes. *International Journal of Intelligent Engineering and Systems* 14(3): 11-22. <http://doi.org/10.22266/ijies2021.0630.02>
- Raj A, Misra JP, Khanduja D (2022) Modeling of wire electro-spark machining of inconel 690 superalloy using support vector machine and random forest regression approaches. *Journal of Advanced Manufacturing Systems* 21(03): 557-571. <https://doi.org/10.1142/S0219686722500196>
- Rehman A, Harouni M, Karchegani NHS, Saba T, Bahaj SA, Roy S (2022) Identity verification using palm print microscopic images based on median robust extended local binary pattern features and k-nearest neighbor classifier. *Microscopy research and technique* 85(4): 1224-1237. <https://doi.org/10.1002/jemt.23989>
- Saidi IA, Rziza M, Debayle J (2021) A novel texture descriptor: circular parts local binary pattern. *Image Analysis and Stereology* 40(2):105-114. <https://doi.org/10.5566/IAS.2580>

Wei Z, Zhang X (2021) Feature extraction and retrieval of e-commerce product images based on image processing. *Traitement du Signal* 38(1):181-190.

<https://doi.org/10.18280/ts.380119>

Xia G, Chen J, Tang X, Zhao L, Sun B (2022) Shift quality optimization control of power shift transmission based on particle swarm optimization–genetic algorithm. *Proceedings of the Institution of Mechanical Engineers, Part D: Journal of Automobile Engineering* 236(5): 872-892.

<https://doi.org/10.1177/09544070211031132>

Yu H, Zheng M, Zhang W, Nie W, Bian T (2022) Optimal design of helical flute of irregular tooth end milling cutter based on particle swarm optimization algorithm. *Proceedings of the Institution of Mechanical Engineers, Part C. Journal of mechanical engineering science* 236(7): 3323-3339. DOI:

<http://doi.10.1177/09544062211042052>

Zhang C, Zhao S, Yang Z, He Y (2023) A multi-fault diagnosis method for lithium-ion battery pack using curvilinear Manhattan distance evaluation and voltage difference analysis. *Journal of Energy Storage* 67:

107575-107575. <https://doi.org/10.1016/j.est.2023.107575>